Volume 18, Number 2, 2025. pp. 131-140

Jordan Journal of Physics

ARTICLE

Shell Model Calculations of Nuclear Properties in (^{91,93}Sr) Strontium Isotopes Using NuShellX@MSU Code

F. H. Obeed[a] and **A. K. Hasan**[b]

[a] *Department of Physics, Faculty of Education for Girls, University of Kufa, Najaf, Iraq.*
[b] *College of Health and Medical Technology, University of Alkafeel, Iraq.*

Doi: **https://doi.org/10.47011/18.2.3**
Received on: 02/09/2023; *Accepted on: 16/04/2024*

Abstract: The nuclear shell model has been applied to calculate various nuclear properties of the ^{91,93}Sr isotopes, including spins and parities, energy spectra, reduced electromagnetic transition possibilities (electric quadrupole and magnetic dipole), magnetic dipole moments, nuclear charge distributions, and mass density as functions of the radial distance from the nucleus center (r). In this study, the NuShellX@MSU code was employed using Gloeckner-Bare G-matrix interaction, within the Gloeckner model space of the orbits ($2p_{1/2}$,$1g_{9/2}$) and ($3s_{1/2}$,$2d_{5/2}$) for protons and neutrons, respectively. The results showed good agreement with the available experimental data (spins and parities of energy spectra) and a confirmation of most levels. Theoretically, new values have been expected for the most nuclear properties, including spin, parities, energy spectra, transition strengths, electric quadrupole, dipole magnetic moments, the nuclear charge, and mass density distributions. Previously, these accounts had not been determined empirically.

Keywords: Energy spectra, Transition strengths, Density distributions.

1. Introduction

The nuclear shell model has been one of the central theoretical keys for interpreting nuclear structure experimental data. Due to the significant growth in Hilbert space dimensions, practical calculations must be carried out in a reduced Hilbert space, known as the model space. Accordingly, effective interactions, such as Gloeckner (Gl) and Gloeckner Pulse bare G-Matrix (Glb), have been designed to fit the space of the chosen model. In these interactions, the shell model has succeeded to describe many properties of the nuclei, including the magic number, spin, valence, binding energy of the nucleus, the cross-section of the neutron captured by the nuclei, and the transmission probabilities of gamma-ray emission from the nuclei, as well as electric quadrupole and dipole magnetic moments [1, 2]. Isotopes around the closed proton and neutron shells (^{88}Sr isotope) play a key role in nuclear physics [3]. Strontium nucleus (^{38}Sr) has four stable, naturally occurring isotopes: ^{84}Sr (0.56%), ^{86}Sr(9.86%), ^{87}Sr(7.0%), and ^{88}Sr (82.58%). Thirty-two unstable isotopes of strontium are known to exist, ranging from ^{73}Sr to ^{108}Sr [4,5]. A large number of studies presented that nuclei in $A \geq 90$ for semi-magic shell closure ($Z = 38$ and $N = 50$) mass region provide suitable objects to investigate the structure level. Many properties of these nuclei have been interpreted in shell-model calculations above the closed core nucleus ^{88}Sr.

Several researchers have contributed to this field. Ahalpara and Bhatt explained the shell-model spectra of ^{92}Tc and ^{93}Ru nuclei [3]. Gloeckner described the nuclear shell model calculations for zirconium and niobium isotopes

Corresponding Author: F. H. Obeed **Email**: fatimahh.alfatlawi@uokufa.edu.iq

with proton filling ($2p_{1/2}$, $1g_{9/2}$) and ($3s_{1/2}$, $2d_{5/2}$) orbits [6]. Several of ^{92,93,94,95}Zr isotopes' properties, including energy spectra, have been well described in shell-model calculations using ($2p_{1/2}$,$1g_{9/2}$) and ($3s_{1/2}$,$2d_{5/2}$) space by many researchers, including Fotiades *et al*. [7]. Wei *et al.* proposed a new high-spin level scheme for the ^{87}Sr nucleus based on coupling a $g_{9/2}$ neutron hole to the yrast states of the ^{88}Sr core, which accounts for its observed energy states [8]. Li *et al*. calculated high-spin states in the semi-magic nucleus ^{89}Y and studied neutron-core excitations in N = 50 isotones [9]. Furthermore, Wu *et al*. performed shell-model calculations of core-excited level structures for the ^{89}Sr nucleus using the NuShellX code [10]. Sihotra *et al.* studied the wave functions for the excited higher-spin states of the ^{96}Tc nucleus utilizing the jj45pn model space of valence protons distributed over the single-particle $2p_{1/2}$ and $1g_{9/2}$ orbitals and neutrons occupying $1g_{7/2}$, $2d_{5/2}$, $2d_{3/2}$, $3s_{1/2}$, and $h_{11/2}$ orbitals [11]. Obeed studied the high-spin states for the ^{90,91,92}Y isotopes by applying nuclear shell model calculations with the OXBASH code [12].

The aim of the present work is to describe some of the nuclear structure properties by increasing the number of valence nucleons (neutrons) outside the closed ^{88}Sr nucleus of ^{91,93}Sr isotopes by using the NuShellX@MSU code with Gloeckner interaction and Bare G-matrix.

2. Theory

Understanding the properties of nuclei, such as energy levels, wave functions, the description of electromagnetic transition rates, electric quadrupole and dipole magnetic moments, and nucleon density distributions, is the key problem in nuclear physics. Therefore, many models have been developed to solve this problem and establish the structure of the nucleus [13, 14]. A successful description of these properties depends critically on the choice of model space and effective interactions. Through these inputs, the reduced one-body matrix elements can specify the shell-model wave functions of initial spin J_i and final spin J_f for a given multipolarity λ. This can be extracted as a linear combination of single-particle matrix elements [12, 15, 16]:

$$\langle \mathrm{NITT_z}\|\mathrm{O}(\lambda)\|\mathrm{NITT_z}\rangle = \sum_{\rho\rho'}\langle\rho|\mathrm{O}(\lambda,\mathrm{M})|\rho'\rangle\, \mathrm{D}^{\mathrm{NITT_z}}(\lambda,\rho,\rho') \quad (1)$$

where $\langle\rho|\mathrm{O}(\lambda,\mathrm{M})|\rho'\rangle$ are the single-particle matrix elements.

When the operator mediates the observable quadrupole electrical elements of a many-body nuclear state $|\mathrm{NITT_z}\rangle$, it can be represented as a sum of one-body operators. The one-body factor O in the nuclear shell model can be represented in the second quantitative formula as:

$$\mathrm{O} = \sum_{K=1}^{A} O_K = \sum_{\rho\rho' \mathrm{mm}'} \langle \rho\mathrm{m}|\mathrm{O}|\rho'\mathrm{m}'\rangle\, a^{+}_{\rho\mathrm{m}} a_{\rho'\mathrm{m}'} \quad (2)$$

Here, the first summation acts on all nucleons, while the second summation acts on all energetic single-particle states $|\rho\mathrm{m}\rangle = |njlmtt_z\rangle$ in the fundamental space of the shell model, and the $a^{+}_{\rho\mathrm{m}}$ and $a_{\rho'\mathrm{m}'}$ A spherical tensor of order λ. In the coordinate space, O = O(λ.,M),

$$\mathrm{D}^{\mathrm{NITT_z}}(\lambda,\rho,\rho') = \frac{\langle \mathrm{NITT_z}\|\left[\mathrm{a}^{\dagger}_{\rho}\times \mathrm{a}_{\rho'}\right]^{\lambda}\|\mathrm{NITT_z}\rangle}{\sqrt{2\lambda+1}} \quad (3)$$

through the appropriate algebraic operations on the model wave functions.

Low-lying levels of even-odd nuclei typically decay via electric quadrupole (E2) and magnetic dipole (M1) transitions to lower yrast levels. The reduced transition probability for a generic multipolar electromagnetic transition is given by [15, 16]:

$$\mathrm{B}(\sigma\lambda;\ \mathrm{J_iT_iT_z} \longrightarrow \mathrm{J_iT_iT_z}) = \frac{1}{2\mathrm{J_i}+1}\left|\langle \mathrm{J_fT_fT_z}\|\mathrm{O}^{\sigma\lambda}\|\mathrm{J_iT_iT_z}\rangle\right|^2 \quad (4)$$

Specifically, the reduced electric and magnetic transition probabilities are expressed as:

$$\mathrm{B}(\mathrm{E1};\ \mathrm{J_iT_iT_z} \longrightarrow \mathrm{J_iT_iT_z}) = \frac{1}{2\mathrm{J_i}+1}\left|\langle \mathrm{J_fT_fT_z}\|\mathrm{O}^{\mathrm{E1}}\|\mathrm{J_iT_iT_z}\rangle\right|^2 \quad (5)$$

and

$$\mathrm{B}(\mathrm{M1};\ \mathrm{J_iT_iT_z} \longrightarrow \mathrm{J_iT_iT_z}) = \frac{1}{2\mathrm{J_i}+1}\left|\langle \mathrm{J_fT_fT_z}\|\mathrm{O}^{\mathrm{M1}}\|\mathrm{J_iT_iT_z}\rangle\right|^2 \quad (6)$$

Here, $\mathrm{O}^{\sigma\lambda}$ refers to a multipolar electromagnetic operator of rank λ, often analogous in form to the matrix of the residual interaction between nucleons.

Among nuclear moments, the quadrupole moment has been particularly challenging to measure accurately, although it provides vital information about the deformation of the nucleus [18]. The spectroscopic quadrupole moment

Q_s of a nuclear state, along with its total angular momentum J, gives insight into the deviation of the charge distribution from spherical symmetry—particularly relevant in nuclei with non-zero projection of angular momentum (K = 0). For a given nucleus, the effective charges of the proton and neutron can be used in shell model calculations to find the quadrupole moments [15, 18, 19]. The spectroscopic electric quadrupole moment can be directly connected to the intrinsic quadrupole moment Q′ by the expression [15, 20]:

$$Q_s(JK) = \frac{3K^2 - J(J+1)}{(2J+3).(J+1)} Q' \quad (7)$$

$Q_s > 0$ indicates a prolate deformation for the isotope. $Q_s < 0$ indicates an oblate deformation for the isotope. $Q_s = 0$ corresponds to an isotope with spherical shape [20]

$$Q' = \sqrt{\frac{16\pi}{5}}.(B(E2))^{1/2} \quad (8)$$

Here, K is the estimation of the total angular momentum of the nucleus along the deformation axis.

The one-body density factor can be transformed into two-body density as the following change [15]:

$$\hat{\rho}(\vec{r}) = \sum_{i=1}^{A} \delta(\vec{r} - \vec{r}_i) \quad (9)$$

The equations of the nuclear charge and mass density can be described as follows:

$$\int \rho_{\circ}(r)\ d\tau = 4\pi \int \rho_{\circ}(r)\ r^2 dr = A \quad (10)$$

where A denotes the nucleus mass number.

The distribution of the nuclear charge density can be explained by the equation:

$$\int \rho_{ch}(r)\ d\tau = 4\pi \int \rho_{ch}(r)\ r^2 dr = z \quad (11)$$

3. Results and Discussion:

The NuShellX@MSU code was implemented by using Gloeckner interaction with Bare G-matrix. The Gloeckner (gl) space model was applied for the deformed orbitals ($2p_{1/2}$, $1g_{9/2}$) and ($3s_{1/2}$, $2d_{5/2}$) of the proton and neutron of the valence particles (three and five neutrons) for ^{91}Sr and ^{93}Sr isotopes, respectively. Valence particles that have determined several nuclear properties are distributed outside $^{88}_{38}Sr$ closed core nucleus. These properties include energy spectra and nuclear states (i.e., total angular momentum and parity). The transition probabilities of the electric quadrupole B(E2) and magnetic dipole B(M1), as well as the nuclear charge distribution $\rho_{ch}(r)$ and mass density $\rho_m(r)$, are functions of the radial distance r from the center of the nucleus and are influenced by the electric and magnetic quadrupole and dipole moments.

The NuShellX@MSU code has been used to compute exact energy levels, eigenvectors, and spectral overlaps of the low-lying states in the Hamiltonian matrix. These large-scale shell model calculations utilize a proton–neutron coupled basis in total angular momentum J, with matrix dimensions reaching up to 100 million [21].

The Skyrme SLy4 interaction was applied to calculate radial wave functions for the single-particle matrix elements. These calculations were performed using the NuShellX@MSU code, incorporating effective nucleon charges and gyromagnetic factors g**,** where g represents the values of orbital parameters and effective spin factors (g) $\{g_s(p), g_s(n), g_l(p), g_l(n)$. The single-particle energy levels for the valence nucleons, as calculated by NuShellX@MSU, are $\{\varepsilon_{2p1/2}(p)$ = -7.124 MeV, $\varepsilon_{1g9/2}(p)$ = -6.248, $\varepsilon_{3s1/2}(n)$ = -5.506 MeV, and $\varepsilon_{2d5/2}(n)$ = -6.338 MeV$\}$. The following section presents and discusses the results obtained for each isotope.

3.1 Energy Levels

1. *^{91}Sr isotope:*

This isotope consists of three valence neutrons occupying the $3s_{1/2}$ and $2d_{5/2}$ orbitals above the $^{88}_{38}Sr$ closed nucleus. The calculated and experimental energy spectra for ^{91}Sr are compared in Fig. 1 [22]. The ground-state energy, spin, and configuration from the present calculations agree well with the available experimental data [22].

In the present results, the experimental energy level at 0.0936^{+4}_{-4} MeV [22] is confirmed to have total angular momentum (3/2), although no spin assignment had been made experimentally. Additionally, the calculated results confirm the spin-parity assignments of two experimental energy levels: $\{1.042^{+25}_{-25}$ and $1.23^{+5}_{-5}\}$. These assignments were not previously determined in experimental data [22].

The experimental level at 2.657^{+6}_{-6} [22], previously known to have positive parity (but no spin), is now confirmed as 9/2. Furthermore, it has been affirmed experimentally [22] with the value of 2.077^{+15}_{-15}. The calculated states $\{5/2^+, 3/2^+ and\ 7/2^+\}$ have been predicted with the values (1.36^{+7}_{-7},1.482^{+10}_{-10} and 1.917^{+12}_{-12}), but are experimentally unknown in states [22].

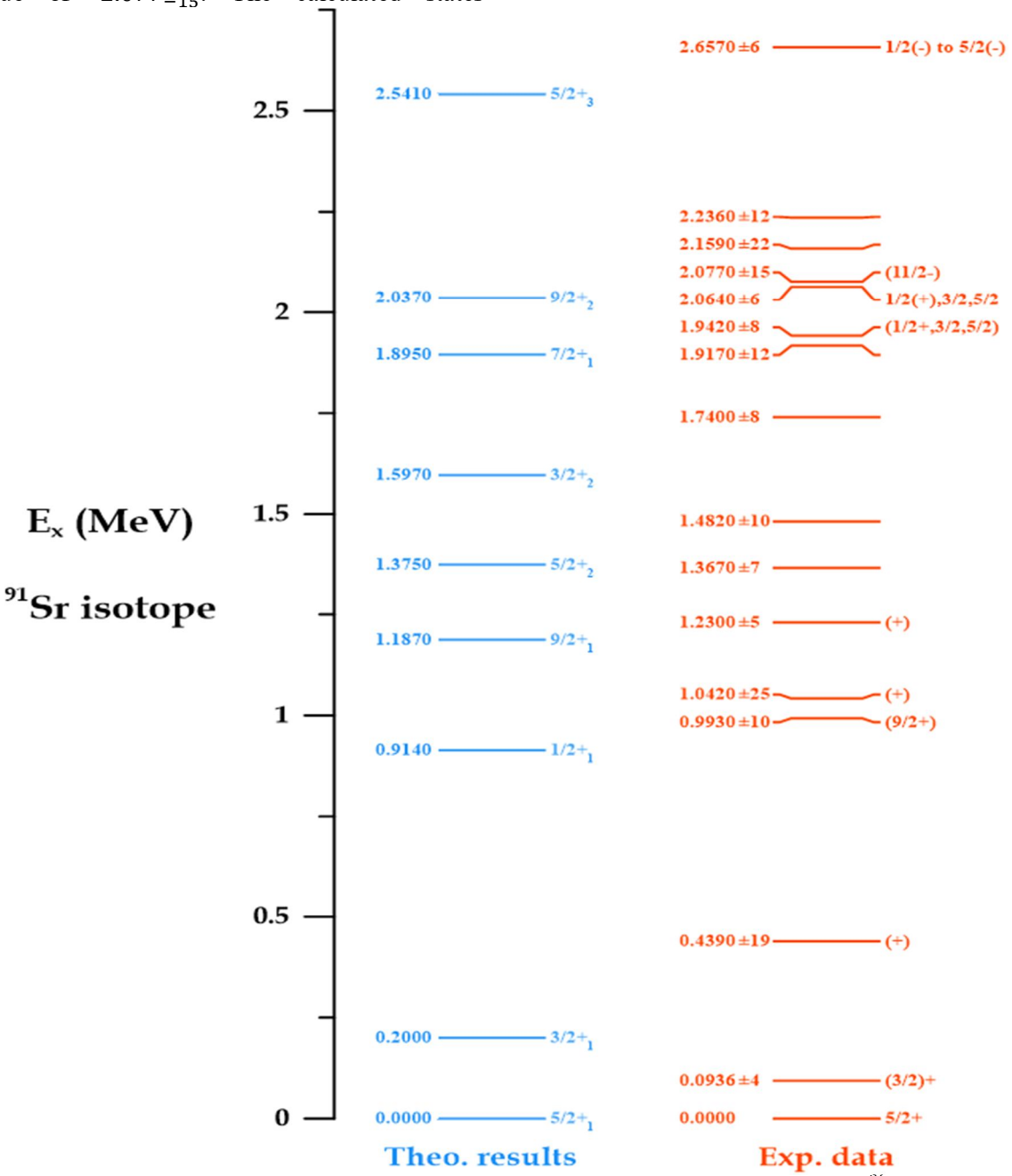

FIG. 1. Comparison of theoretical results with experimental data for the energy values for the ^{91}Sr isotope using glb interaction. The experimental data are adopted from Ref. [22].

2. ^{93}Sr isotope:

This isotope contains five nucleons (neutrons) occupying the ($3s_{1/2}$, $2d_{5/2}$) orbitals above the $^{88}_{38}$Sr closed-core nucleus. The calculated and experimental spectra values [23] for the ^{93}Sr isotope are displayed in Fig. 2 and can be interpreted as follows:

The energy value for the ground state, along with its spin and valence, is well reproduced from the experimental values [23]. The predicted theoretical states $\{3/2^+, 5/2^+, 7/2^+, 9/2^+, 5/2^+$ and $9/2^+\}$ have been confirmed for the experimental energy values $\{1.142^{+4}_{-4}, 1.148^{+6}_{-6}, 1.562^{+9}_{-9}, 1.808^{+6}_{-6}, 2.141^{+11}_{-11},$ and 2.351^{+11}_{-11} MeV.

There is no available experimental energy value to compare with the newly predicted theoretical energy level of 0.739 for the state $1/2^+$. The expected theoretical state $3/2^+$ has been specified for the experimental energy level 1.910^{+9}_{-9} MeV, but not for the experimental data. For the energy levels of ^{91,93}Sr isotopes, the experimental value was higher than the theoretical maximum value for our isotope calculations: 2.541 MeV of the $5/2^+_3$ state and 2.389 MeV of the $9/2^+_2$ state, respectively. Therefore, there are several experimental values that were not compared with our theoretical values.

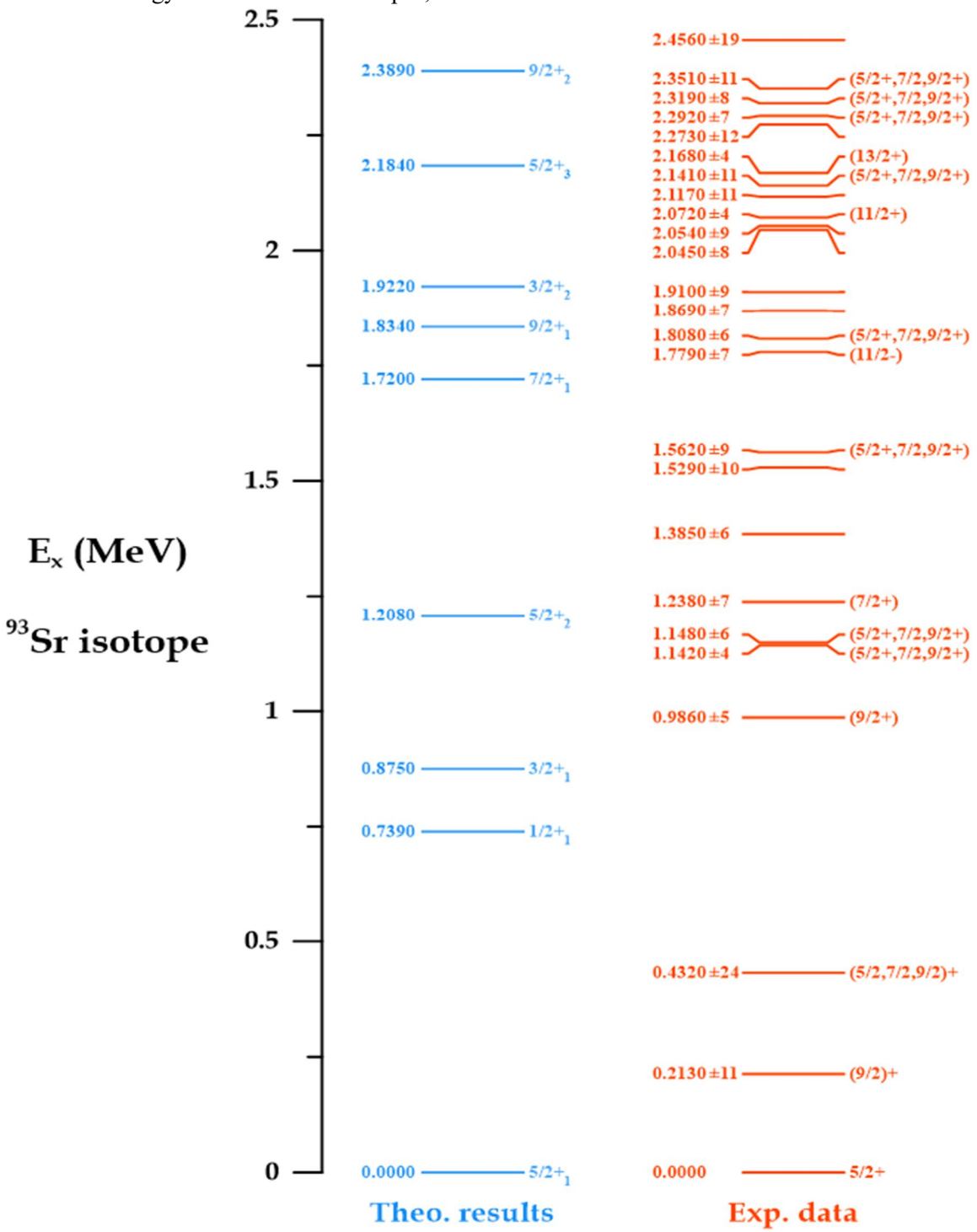

FIG. 2. Comparison of theoretical results with experimental data for the energy values for the ^{93}Sr isotope using glb interaction. The experimental data are adopted from Ref. [23].

3.2 Reduced Electric Quadrupole and Magnetic Dipole Transition Probabilities

In our calculations, the NuShellX@MSU code was also applied to generate the one-body transition density matrix (OBDM) elements using Gloeckner interaction with Bare G-matrix. These interactions took place in the orbits of the Glockner space model, namely, ($2p_{1/2}$, $1g_{9/2}$) and ($3s_{1/2}$, $2d_{5/2}$) for protons and neutrons, respectively. The wave functions of the single-particle matrix elements were estimated for the two isotopes using the Skyrme29 potential, with the following effective nucleon charges for protons and neutrons: {(e_p = 1.622e,e_n = 1.244e); (e_p = 1.5e,e_n = 1.720e)}. The values of the orbital parameters and effective spin factors (g){$g_s(p)$, $g_s(n)$, $g_l(p)$, $g_l(n)$ were equal to (5.027, -3.443, 1.418, 0.418); (5.027, -3.443, 1.474, 0.474) } and were used to conduct the magnetic dipole B (M1) for the ^{91,93}Sr isotopes, respectively.

The theoretical values for the transition probabilities of the electric quadrupole and the magnetic dipole in the Sky29 potential with nucleons of effective charges (protons and neutrons) for ^{91,93}Sr isotopes are shown in Tables 1 and 2, respectively. Table 1 explains E2 and M1 transition strengths for the ^{91}Sr isotope. The computed B(E2) transition probabilities show good agreement with the experimental data [22], particularly for the strong E2 decays from states $3/2_1^+$ to $5/2_1^+$, with a theoretical value of 362.3 (e^2fm^4) and 42.33×10^{-5} (μ_N^2) for the electric quadrupole and magnetic dipole transitions, respectively. These results were compared with the experimental values, which were reported as > 340.8 (e^2fm^4) and < 2.148×10^{-5} (μ_N^2). However, the M1 transition strength remains unconfirmed experimentally.

For the ^{93}Sr isotope, the theoretical E2 and M1 transition strengths are listed in Table 2. These values do not yet have corresponding experimental data for comparison [23]. Several new electromagnetic transitions for B(E2;↓) and B(M1;↓) have been computed applying the NuShellX@MSU code with Glb interaction for ^{91,93}Sr isotopes, illustrated in Tables 1 and 2. These predicted transitions, currently unobserved experimentally, contribute additional theoretical insights into the energy levels and electromagnetic properties of these isotopes.

TABLE 1. Comparison of experimental and theoretical values for electric quadrupole and magnetic dipole transition probabilities for positive-parity spin states in the ^{91}Sr isotope. The experimental data are adopted from Ref. [22].

	Theoretical Results		Experimental Results		
$J_i \rightarrow J_f$	$(BE2\downarrow)(e^2fm^4)$	$(BM1\downarrow)(\mu_N^2))$	Multi-polarity	$(BE2\downarrow)(e^2fm^4)$	$(BM1\downarrow)(\mu_N^2))$
$3/2_1^+ \rightarrow 5/2_1^+$	362.3	42.33×10^{-5}	E2(+M1)	> 340.8	<2.148× 10^{-5}
$1/2_1^+ \rightarrow 5/2_1^+$	96.47	-----	-----	-----	-----
$1/2_1^+ \rightarrow 3/2_1^+$	25.18	-----	-----	-----	-----
$9/2_1^+ \rightarrow 5/2_1^+$	84.68	-----	-----	-----	-----
$7/2_1^+ \rightarrow 5/2_1^+$	215.8	-----	-----	-----	-----
$7/2_1^+ \rightarrow 3/2_1^+$	78.63	-----	-----	-----	-----
$7/2_1^+ \rightarrow 9/2_1^+$	161.9	1.61×10^{-2}	-----	-----	-----

TABLE 2. Comparison of experimental and theoretical values for electric quadrupole and magnetic dipole transition probabilities for positive-parity spin states in the ^{93}Sr isotope. The experimental data are adopted from Ref. [23].

	Theoretical Results		Experimental Results		
$J_i \rightarrow J_f$	$(BE2\downarrow)(e^2fm^4)$	$(BM1\downarrow)(\mu_N^2))$	multi-polarity	$(BE2\downarrow)(e^2fm^4)$	$(BM1\downarrow)(\mu_N^2))$
$1/2_1^+ \rightarrow 5/2_1^+$	25.03	-----	-----	-----	-----
$3/2_1^+ \rightarrow 5/2_1^+$	571	-----	-----	-----	-----
$3/2_1^+ \rightarrow 1/2_1^+$	111	-----	-----	-----	-----
$7/2_1^+ \rightarrow 5/2_1^+$	582.9	-----	-----	-----	-----
$7/2_1^+ \rightarrow 3/2_1^+$	183.5	-----	-----	-----	-----
$7/2_1^+ \rightarrow 5/2_2^+$	0.8489×10^{-2}	-----	-----	-----	-----
$9/2_1^+ \rightarrow 5/2_1^+$	88.45	-----	-----	-----	-----
$9/2_1^+ \rightarrow 5/2_2^+$	40.52	-----	-----	-----	-----
$9/2_1^+ \rightarrow 7/2_1^+$	26.76	-----	-----	-----	-----

3.3 Electric Quadrupole and Magnetic Dipole Moments

The electric quadruple moments (Q_s) and magnetic dipoles (μ) of the ^{91,93}Sr isotopes have been calculated and are presented in Table 3, which compares the theoretical values with the experimental data [22, 23] for the two isotopes used in this study. The calculations show that the quadrupole moments of ^{91}Sr isotope in the states {$5/2_1^+$, $9/2_1^+$, $3/2_2^+$, $7/2_1^+$, $9/2_2^+$, and $5/2_3^+$} have negative signs (oblate shape dominance), while for the ^{93}Sr isotope, the states {$5/2_1^+$, $7/2_1^+$, $9/2_1$, $3/2_2^+$, and $5/2_3^+$ } of the quadrupole moments have appeared with positive signs (prolate shape dominance), whereas the states {$3/2_1^+$, $5/2_2^+$, and $9/2_2^+$} exhibit negative signs, representing the oblate shape dominance.

The calculated magnetic dipole moments (μ) of the ground state $5/2_1^+$ are -0.889 μ_N and -0.792 μ_N for ^{91,93}Sr isotopes. These values agree with the corresponding experimental results {0.885^{+2}_{-2} and -0.7926^{+12}_{-12}}. Additionally, the calculated quadrupole moment of 25.81(efm^2) for ^{93}Sr matches well with the experimental value of {$+25.8^{+11}_{-11}$} efm^2. The remaining quadrupole (Q_s) and magnetic dipole (μ) moments have been predicted theoretically but have not yet been confirmed experimentally.

TABLE 3. Comparison of experimental [22, 23] and theoretical values for the quadrupole with magnetic dipole moments in ^{91,93}Sr isotopes using glb interaction.

Isotopes		Theoretical Results		Experimental Results	
	J^π	$(Q)(efm^2)$	$\mu(\mu_N)$	$(Q)(efm^2)$	$\mu(\mu_N)$
^{91}Sr isotope	$5/2_1^+$	-1.62	-0.889	4.2 ±11	-0.885± 2
	$3/2_1^+$	14.59	-0.397	-----	-----
	$1/2_1^+$	0	-1.722	-----	-----
	$9/2_1^+$	-5.73	-1.614	-----	-----
	$5/2_2^+$	2.35	-2.302	-----	-----
	$3/2_2^+$	-6.69	0.261	-----	-----
	$7/2_1^+$	-14.47	-0.039	-----	-----
	$9/2_2^+$	-10.06	-3.119	-----	-----
	$5/2_3^+$	-9.19	-1.011	-----	-----
^{93}Sr isotope	$5/2_1^+$	25.81	-0.792	+25.8±11	-0.7926±12
	$1/2_1^+$	0	-1.722	-----	-----
	$3/2_1^+$	-32.17	0.167	-----	-----
	$5/2_2^+$	-20.18	-2.164	-----	-----
	$7/2_1^+$	20.06	0.136	-----	-----
	$9/2_1^+$	32.92	-2.912	-----	-----
	$3/2_2^+$	21.23	-0.155	-----	-----
	$5/2_3^+$	6.09	-0.931	-----	-----
	$9/2_2^+$	-11.04	-1.440	-----	-----

3.4 Nuclear Charge and Mass Density Distributions

The nuclear charge and mass density distributions of the ^{91,93}Sr isotopes have been computed by implementing the NuShellX @MSU code and sky29 potential as displayed in Figs. 3 and 4 for the above isotopes, respectively. For the ^{91,93}Sr isotopes, the nuclear charge density at the center of the nucleus was found to be ρ_{ch} = 0.08072 Ze/fm^{-3} and ρ_{ch} = 0.0828Ze/fm^{-3}, respectively. These values remain stable at a distance of r = 0.1 fm, as shown in Figs. 3 and 4. At r = 0.2 fm, the charge density begins to decrease, reaching values of ρ_{ch} = 0.08063Ze/fm^{-3} for ^{91}Sr and ρ_{ch} = 0.08346 Ze/fm^{-3} for ^{93}Sr. Beyond these points, the charge density continues to decline gradually until it reaches zero at r = 6.9 fm in both isotopes. Similarly, the nuclear mass density at the center of the nucleus is calculated as ρ_m = 0.1628 nucleon/fm^{-3} for ^{91}Sr and ρ_m = 0.1656 nucleon/fm^{-3} for ^{93}Sr, with a slight increase at r = 0.1 fm. As r increases to 0.2 fm, the mass density also increases slightly to ρm = 0.1631 nucleon/fm^{-3} for ^{91}Sr and ρ_m = 0.1659 nucleon/fm^{-3} for ^{93}Sr. For the ^{91}Sr isotope, the mass density distribution gradually increases, reaching a maximum value of ρ_m = 0.1701 nuclei/fm^{-3} at distances between r = 1.3 and 1.4

fm. Beyond this point, it gradually decreases until it reaches zero at r = 7.3 fm. The nuclear mass density of the ^{93}Sr isotope continues to increase gradually at distances from 0.2 to 1.4 fm, and also at the distance r = 1.5 fm, after which the mass density distribution of this isotope begins to decrease until it stabilizes at zero (r = 7.2 fm). As for the experimental values of the nuclear charge and mass density distributions for the $^{91.93}$Sr isotopes, no ratios have been determined.

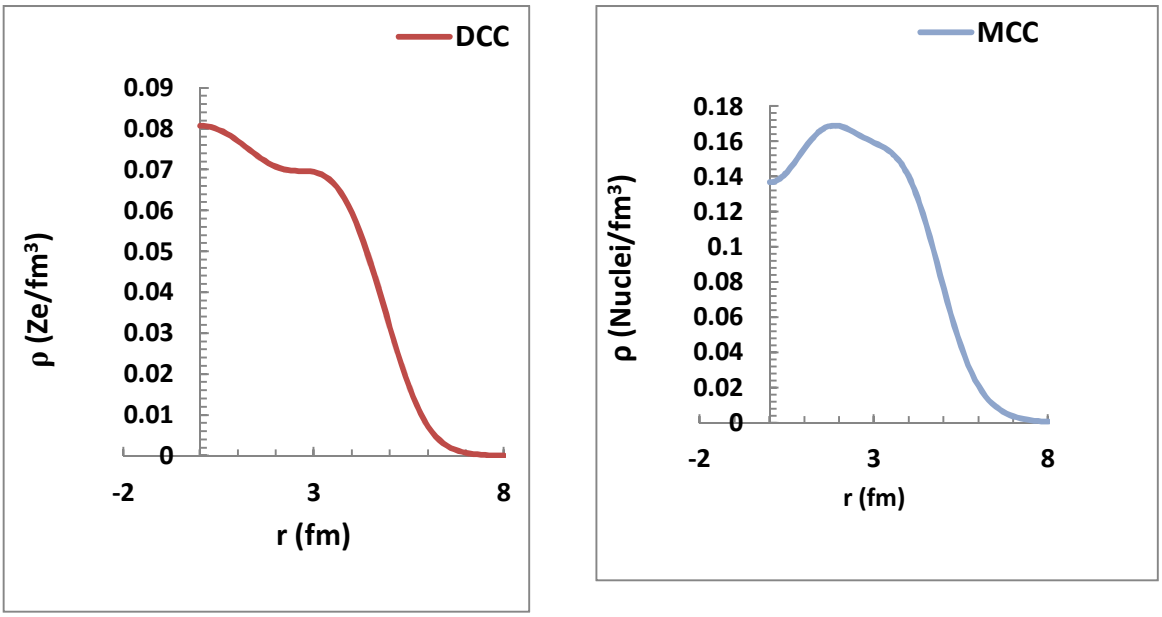

FIG. 3. Nuclear charge and mass density distributions as functions of the radial distance from the center of the nucleus (r) in ^{91}Sr isotope.

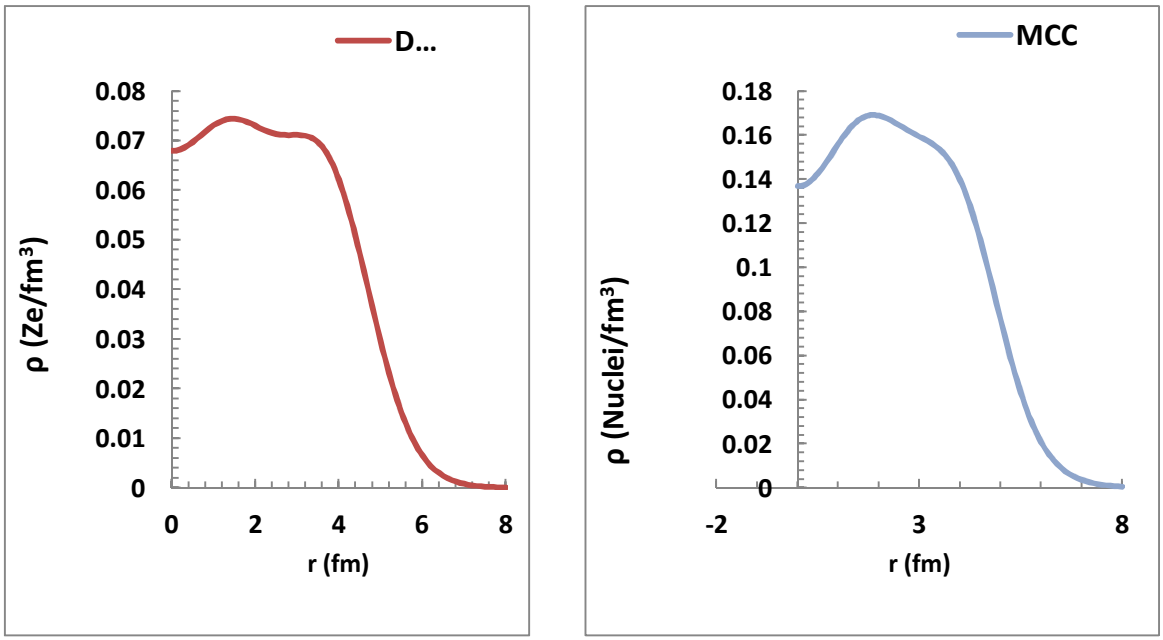

FIG. 4. Nuclear charge and mass density distributions as functions of the radial distance from the center of the nucleus (r) in ^{93}Sr isotope.

4. Conclusions

Through the calculated results of the nuclear properties studied in this manuscript for the ^{91,93}Sr isotopes, and by comparing these characteristics with the experimental data, the following conclusions can be drawn:

- The energy value of the ground state with spin and parity has been well reproduced with the experimental values for both isotopes (^{91}Sr and ^{93}Sr).
- The total angular momentum with parity has been confirmed and determined for some experimental data values of ^{91,93}Sr isotopes.
- Several theoretical energy levels of the ^{91,93}Sr isotopes do not have corresponding values in the experimental data.
- There are experimental energy levels whose values exceed the theoretical maximums calculated in this study: 2.541 MeV for the $5/2_3^+$ state in ^{91}Sr and 2.389 MeV for the $9/2_2^+$ state in ^{93}Sr.
- For the ^{91}Sr isotope, good agreement has been achieved between the calculated magnetic transition probabilities (quadrupole and dipole) and the experimental values, particularly for the strong transition ($3/2_1^+ \rightarrow 5/2_1^+$).
- Some multipolarity types previously listed in experimental data as (E1), (E1 + M2), or (M1 + E2) for transitions in ^{91}Sr have not been definitively confirmed. However, in this study, these transitions are predicted to be of the E2 and M1 types.
- New electromagnetic transition values have been predicted for both ^{91}Sr and ^{93}Sr isotopes using the NuShellX@MSU code with the GLB interaction. These transitions have not yet been observed experimentally.
- The calculated electric quadrupole and magnetic dipole moments of ^{91}Sr and ^{93}Sr indicate that some nuclear states exhibit oblate shapes, while others show prolate shapes. These shape variations reflect structural sensitivities in the nuclear chart and may vary from one nucleus to another.
- Furthermore, it has been found that shape changes with increasing neutron number may also occur with changes in excitation energy or angular momentum within the same nucleus. These changes are attributed to the rearrangement of orbital configurations or to dynamic structural responses.
- The magnetic dipole moments (μ) for the ground state $5/2_1^+$ in both ^{91}Sr and ^{93}Sr isotopes are consistent with available experimental values. For ^{93}Sr, the predicted moment for the $5/2_1^+$ ground state also agrees well with experimental measurements.
- It has been observed that many new values of the electric quadrupole moments (Q_s) and magnetic dipole moments (μ) have been theoretically predicted, but remain experimentally unconfirmed or underestimated.
- The distribution of the nuclear charge density of the ^{91,93}Sr isotopes is stable at the center of the nucleus, at the value at r = 0.1. Beyond this point, the values of the nuclear charge density distribution gradually decrease until they stabilize at zero. On the contrary, the distribution of the nuclear mass density of the ^{91,93}Sr isotopes also begins at a stable value at r = 0.1, so this distance gradually becomes the value of the nuclear mass density distribution, then these values gradually decrease until they settle at zero over a certain distance, and this behavior in the distribution of nuclear charge and mass density explains that the charge density distributions of ^{91,93}Sr isotopes have behaved well, while the charge density distributions of ^{91,93}Sr isotopes have been in an opposite manner due to the presence of a deviation in the center of the nucleus. The nuclear charge distribution and mass density of the ^{91,93}Sr isotopes have not been compared with practical values because they are not currently available.
- The use of the NuShellX@MSU code with glb interaction and gl model space has been suitable for calculating the nuclear properties of ^{91,93}Sr isotopes reported in this study. For ^{91}Sr, the highest value in the experimental energy spectrum is 2.657^{+6}_{-6} MeV for the 1/2 (-) to 5/2 (-) transition, which can be compared to the theoretical prediction of 2.541 MeV for the $5/2_3^+$ state. For ^{93}Sr, the theoretical maximum energy value is 2.389 MeV at the $9/2_2$ state, while the highest observed experimental energy level is 2.456^{+19}_{-19} MeV.

References

[1] Tsunoda, N., Takayanagi, K., Jensen, M.H., and Otsuka, T., Phys. Rev. C, 89 (3) (2014) 02431.

[2] Browne, F., PhD Thesis, University of Brighton, (2016).

[3] Ahalpara, D.P. and Bhatt, K.H., Pramana J. Phys., 6 (1976) 4.

[4] Dickin, A.P., "Radiogenic Isotope Geology", 3rd Ed., (Cambridge University Press, United Kingdom, 2018) p24.

[5] Reddy, E.K., Robinson, R.G., and Mansfield, C.M., J. Natl. Med. Assoc., 78 (1986) 1.

[6] Gloeckner, D.H., Nucl. Phys. A, 253 (1975) 2.

[7] Fotiades, N., Cizewski, J.A., Becker, J.A., Bernstein, L.A., McNabb, D.P., Younes, W.R.X., Clark, W., Fallon, P., Lee, I.Y., Macchiavelli, A.O., Holt, A., and Hjorth, J.M.H., Phys. Rev. C, 65 (2002) 044303.

[8] Wei, L.I.H., Bin, L.U.J., Sheng, L.I.G., Zheng, Y., He, Y.S., Guang, W.X., Ye, H.C., Liang, X.Q., Jian, L.J., Bo, L.C., Peng, H.S., Long, W.J., Heng, W.Y., Wei, L.P., Yan, M.K., Chuan, X., and Jie, S., J. Chin. Phys. C, 38 (7) (2014) 074004.

[9] Li, Z.Q., Wang, S.Y., Niu, C.Y., Qi, B., Wang, S., Sun, D.P., Liu, C., Xu, C.J., Liu, L., Zhang, P., Wu, X.G., Li, G.S., He, C.Y., Zheng, Y., Li, C.B., Yu, B.B., Hu, S.P., Yao, S.H., Cao, X.P., and Wang, J.L., Phys. Rev. C, 94 (2016) 014315.

[10] Wu, Y.H., Yanma, M.K.Y., Cheng, F., and Cai, X.Y, Pramana. J. Phys., 94 (2020) 53.

[11] Sihotra, S., Trivedi, T., Singh, V., Kumar, A., Singh, N., Singh, R.P., Muralithar, S., Kumar, R., Bhowmik, R.K., and Mehta, D., Proc. DAE Symp. Nucl. Phys., 65 (2021).

[12] Obeed, F.H., Jordan J. Phys., 14 (2021) 1.

[13] Brack, M., Damgaard, J., Jensen, A.S., Pauli, H.C., Strutinsky, V.M., and. Wong, C.Y., Rev. Mod. Phys., 44 (1972) 320.

[14] Yoshinaga, N., Yanase, K., Watanabe, C., and Higashiyama, K., Prog. Theor. Exp. Phys., 2021 (2021) 6.

[15] Brussard, P. and Glaudemans, P., "Shell-Model Applications in Nuclear Spectroscopy", (North Holl and Amesterdam, 1977) p452.

[16] Carchidi, M.V., Aldenthal, B.H., and Brown, B.A., Phys. Rev., 34 (1986) 6.

[17] Abood, S.N., Zahra, N.Z.A., and Najam, L.A., J. Rad. Nucl. Appl., 6 (2021) 1.

[18] Gado, K.A., GJMBR-G Interdisciplinary, 14 (2014) 1.

[19] Mantica, P.F., Crawford, H.L., Pinter, J.S., Stoker, J.B., Utsuno, Y., and Weerasiri, R.R., Phys. Lett. B, 662 (2008) 5.

[20] Raman, S., Nestor, C.W., and Tikkanen, Jr.P., At. Data Nucl. Data Tables, 78 (2001) 1.

[21] Brown, B.A. and Rae, W.D.M., Nucl. Data Sheets, 2014 (2014) 1467.

[22] Baglin, C.M., Nucl. Data Sheets, 114 (2013) 1293.

[23] Baglin, C.M., Nucl. Data Sheets, 112 (2011) 1163.